Material behaviour of a cellular composite undergoing large deformations

F. Bartl, H. Klaus, R. Dallner, O. Huber

Accepted Manuscript

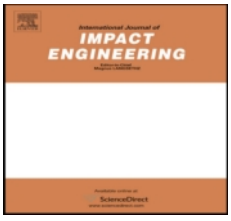

Title: Material behaviour of a cellular composite undergoing large deformations

Authors: F. Bartl, H. Klaus, R. Dallner, O. Huber

PII: S0734-743X(08)00316-3
DOI: 10.1016/j.ijimpeng.2008.11.014
Reference: IE 1727

To appear in: *International Journal of Impact Engineering*

Received Date: 11 December 2007
Revised Date: 24 November 2008
Accepted Date: 24 November 2008

Please cite this article as: Bartl F, Klaus H, Dallner R, Huber O. Material behaviour of a cellular composite undergoing large deformations, International Journal of Impact Engineering (2008), doi: 10.1016/j.ijimpeng.2008.11.014

Material behaviour of a cellular composite undergoing large deformations

F. Bartl [a], H. Klaus [b], R. Dallner [a,*], O. Huber [b],

[a] *Institut für Angewandte Forschung, University of Applied Sciences Ingolstadt, Esplanade 10, 85049 Ingolstadt, Germany*

[b] *Kompetenzzentrum Leichtbau, University of Applied Sciences Landshut, Am Lurzenhof 1, 84036 Landshut, Germany*

Abstract

The intention of this paper is to give an overview of the recent investigations concerning the yield behaviour of a new cellular composite material. This novel material is a syntactic foam with a porous mineral granulate embedded in polyamide. The aim of the investigations is to develop a yield surface suitable for numerical simulations.

To acquire the necessary data for the initial yield surface, a number of different experiments is shown. These experiments include quasi-static uniaxial tension, shear and compression tests as well as hydrostatic tests and experiments with blocked lateral deformations. The evolution of the yield surface into the range of large deformations is investigated and it can be shown that the specific plastic deformation energy is a suitable parameter for the hardening of the material.

To exemplify the capabilities of the material and the material model, a prototype of a crashbox is tested under quasi-static conditions and compared to numerical results.

Key words: material behaviour, cellular composite, finite element method, large deformation, yield surface, multiaxial material tests, crashbox

1 Introduction

A modern engineer is often confronted with the task of designing components with a good ability to absorb energy at almost constant stress together with

* Corresponding author. Tel.: +49-841-9348-239; fax: +49-841-9348-220.
Email address: rudolf.dallner@fh-ingolstadt.de (R. Dallner).

sufficient strength. Cellular materials are one type of material which is suitable for such a component. This fact in combination with a low specific weight makes them a suitable material for designing components relevant for crash applications. The material investigated in this paper is a new cellular composite material. It is a syntactic foam with porous mineral granulates embedded in a cast polyamide matrix (see Fig. 1). The material properties of the investigated cellular composite can be adjusted to the specific use by using suitable matrix- and/or granulate materials [1].

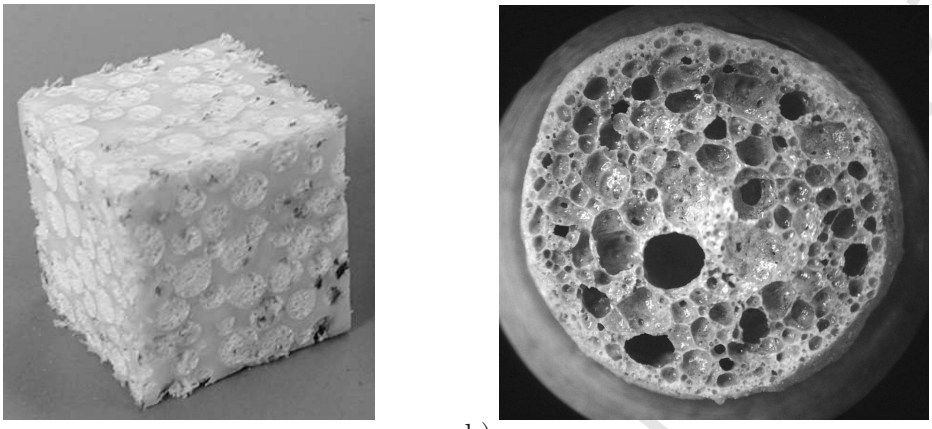

a) b)

Fig. 1. Cellular composite material: a) Granulates in Matrix; b) Cross Section of a single granulate [2]

For the investigated material Dennert Poraver GmbH Schlüsselfeld, Germany, delivered the cellular glass granulates with a diameter between two and four millimeters. The composite is produced by Quadrant engineering plastic products Almelo, Netherlands. Fig. 2 shows the casting process schematically. First the granulates are filled in the form and the form is then shaken to obtain a dense sphere packing of the granulates. After that, the granulate fill is infiltrated with the matrix material.

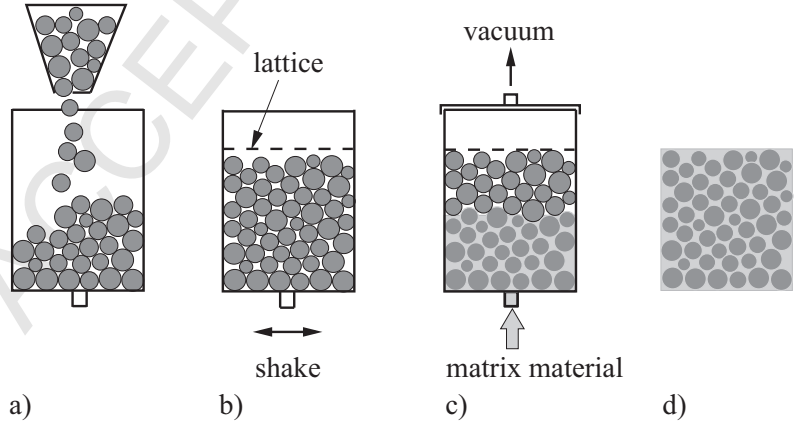

Fig. 2. Composite production - schematically : a) filling of the form with granulates; b) compaction by vibration; c) infiltration of the form; d) cellular composite

The mechanical properties of the cast polyamide PA6 ($\rho = 1.15 g/cm^3$) and the glass foam granulates ($\rho_{average} = 0.37 g/cm^3$) are described in [3]. The mechanical properties of the polyamide (both stiffness and strength) are dependent on the water content and the loading velocity. Experimental investigations of the granulates showed a Young's modulus of $E = 1700 MPa$ and a Poisson's ratio of $\nu = 0.3$. The structure of the composite and the distribution of the glass foam granulates within the matrix were investigated by micro computer tomography analysis (μ-CT analysis) [4]. Fig. 3 shows the results of the μ-CT analysis of a block with the dimensions $66mm \times 45mm \times 45mm$. The average cell diameter is consistent with the average granulate diameter.

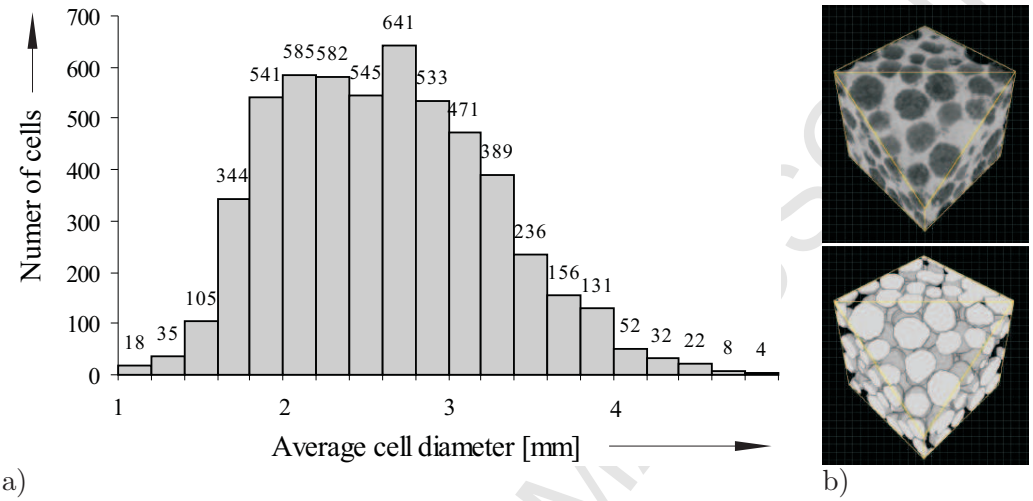

Fig. 3. Micro computer tomography analysis of the composite: a) Average cell diameter; b) Detail of the 3D structure - upper picture: matrix - lower picture: granulates

The μ-CT analysis detected a matrix volume fraction of 50.8% and a granulate volume fraction of 49.2%.

The elastic behaviour of the material was investigated in [5, 6, 7, 8]. It was shown that the specific stiffness and the specific compression strength under uniaxial compression are improved significantly by the cellular granulates up to levels of strains, where the material starts to yield.

In the following the experimental investigations of the elasto-plastic material behaviour of the cellular composite are described. Special emphasis is laid on the description of the yield surface and its evolution into the range of large deformations. The yield behaviour is incorporated into an existing material model [9], *MAT_ BILKHU_DUBOIS_FOAM based on [10], in the FEM software LS-DYNA [11]. This is a prerequisite for numerical simulations, which are an essential part of a modern product development process. The focus of this paper is on quasi-static investigations. However, the strain rate sensitivity of the material may be accounted for, e.g. by appropriate scaling of the quasi-static yield surface [12].

2 Experimental investigations

For all quasi-static tests the cast polyamide was conditioned to 2.5% water content (percent by weight). The tests were carried out with an electromechanical universal material testing machine (Zwick; Z 150). For the axial strain measurement at the surface of the specimen an incremental automatic extensometer (Zwick, MultiXtens) was used. The motorized arms of the extensometer were controlled by the test software (Zwick, testXpert) and allowed a variable gauge length. The test software controlled the test itself and the data acquisition during the test.

The composite has a unique infiltration direction due to the production process (Fig. 2). Uniaxial compression tests in the elastic range were made to investigate the isotropic behaviour of the mechanical properties on the basis of the Young's modulus. Two cubes with an edge length of 70mm were used as specimens, which were loaded between two parallel plates with a constant velocity of $10mm/min$. The extensometer had a gauge length of $50mm$. One specimen was loaded consistent with the infiltration direction, the other one was tested perpendicular to the direction of the infiltration. The Young's modulus was equal in good approximation in both cases. Therefore the composite is considered as quasi-isotropic.

Fig. 4a shows typical stress strain diagrammes of the composite under uniaxial compression. The dimensions of the specimen were 50mm × 50mm × 100mm. The specimens were loaded between two parallel plates with a constant velocity ($\dot{\varepsilon}_{start} = 1 \cdot 10^{-3} s^{-1}$). The strain was measured with the automatic extensometer (gauge length = $50mm$).

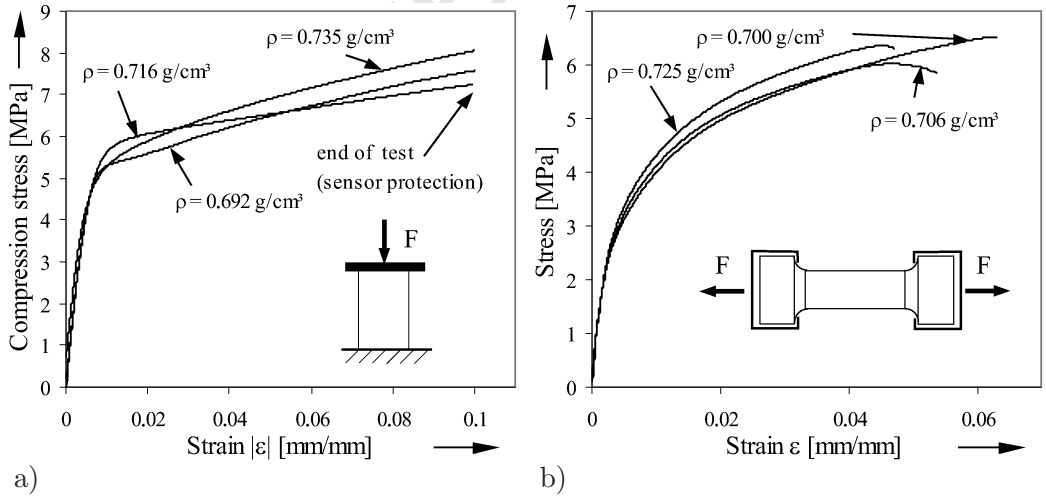

Fig. 4. Quasi-static uniaxial tests: a) compression test; b) tension test

The principle mechanical behaviour of the cellular composite under compression load corresponds to conventional cellular solids. A range of transition

exists between the quasi linear elastic range and the range with low hardening (Fig. 4a).

For the uniaxial tension test (Fig. 4b) the width of the specimen (70mm × 70mm × 250mm) was reduced in its central part over a length of 150mm to a cross section of 45mm × 45mm. The load was transfered to the specimen via form locking. The strain was measured with the automatic extensometer (gauge length = $60mm$). The specimens were loaded with a constant velocity ($\dot{\varepsilon}_{start} = 1 \cdot 10^{-3} s^{-1}$). Fracture occurred at 6% strain. Under uniaxial tension the range of transition was more pronounced than in the uniaxial compression tests.

Fig. 5 shows the experimental setup for the shear test according to DIN 53 294. The vertical angle of the shear specimen was about 4° higher compared to the DIN. Thus the distribution of the shear stress along the specimen is supposed to be more homogeneous [7, 13] (Fig. 5b). The compression forces were transfered through cutting plates at the ends of the specimen (Fig. 5a). The

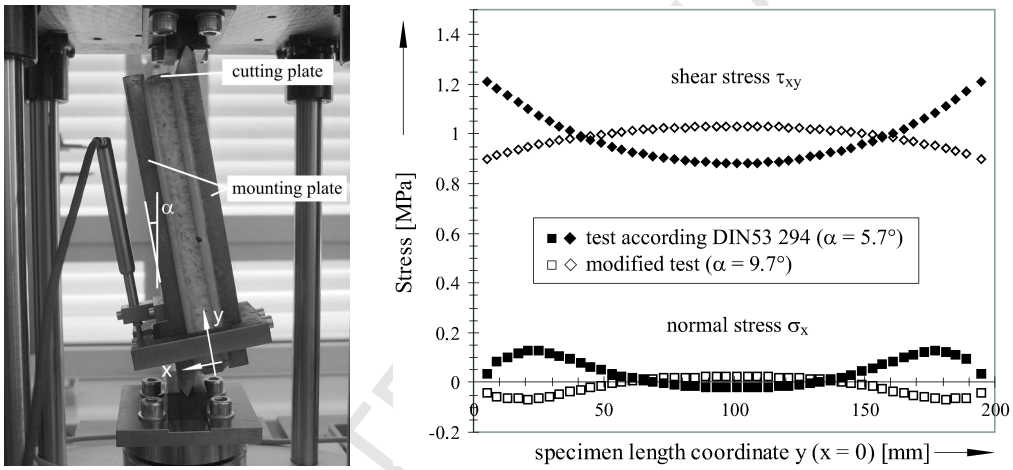

a) b)

Fig. 5. Shear test: a) Experimental setup; b) Numerical Comparison between the test according to DIN and the modified test [7, 13]

dimensions of the specimen were 20mm × 50mm × 200mm. The specimens were loaded with a constant velocity ($\dot{\gamma}_{start} = 1 \cdot 10^{-3} s^{-1}$). The displacement between the two mounting plates was measured with an incremental measuring sensor (Heidenhain, ST3088). Fig. 6 shows the corresponding shear stress strain curves.

Fig. 7 illustrates the failure behaviour of the composite. Under uniaxial compression the polyamide cell walls buckle in an elastic-plastic way and the composite shows a ductile behaviour, whereas the polyamide cell walls break under uniaxial tension at relatively low strains (Fig. 4b, 7b). Pure shear load consists of compression and tension load in the principle axis (Fig. 7c). Therefore the

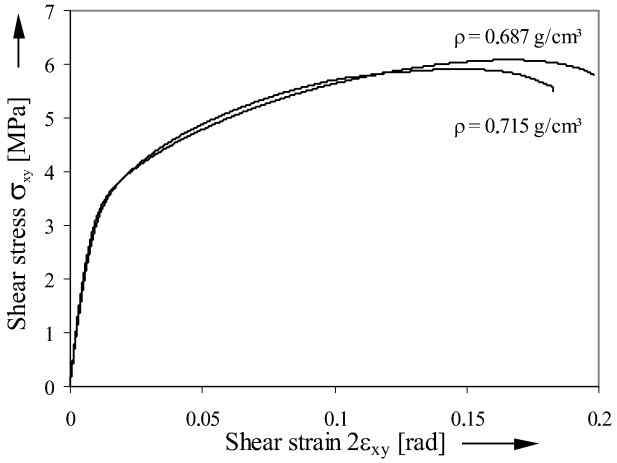

Fig. 6. Shear test: Stress strain curves

material behaviour under uniaxial tension determines the shear behaviour. The shear strength corresponds approximately to the tensile strength (Fig. 4b, 6).

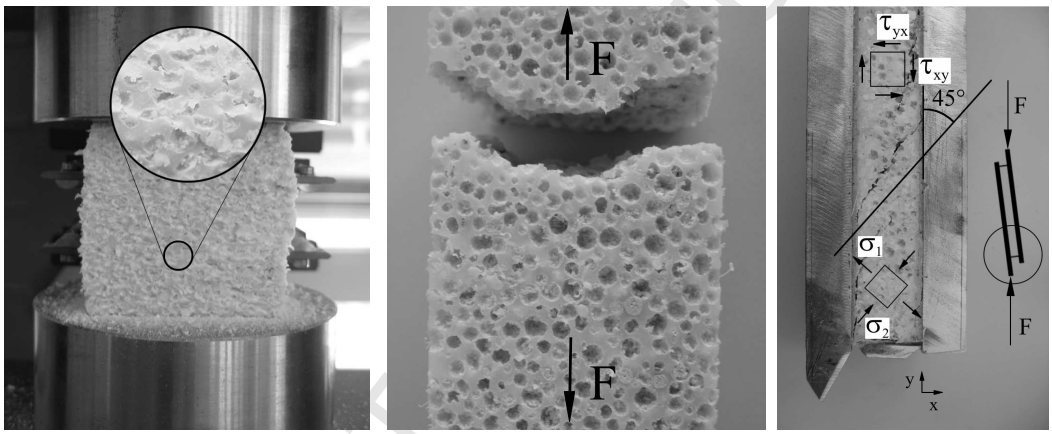

a) b) c)

Fig. 7. Material failure: a) Uniaxial compression; b) Uniaxial tension; c) Pure shear load

Cellular materials as well as cellular composites compact under compression in a different way than materials without porosity. The yield criterion depends on hydrostatic pressure. Therefore a hydrostatic pressure test is essential to investigate this effect on the yield criterion of cellular materials. Loading the specimen through a surrounding fluid is an easy way to create hydrostatic compression. Fig. 8a shows the experimental setup schematically.

Glycerin was used as fluid. The end of the stamp, reaching into the fluid, was conical. Thus the included air spilled out of the pressure chamber with the displaced fluid until the o-ring entered the cylindrical part of the pressure chamber and started to seal. The feed opening and the opening for the stamp

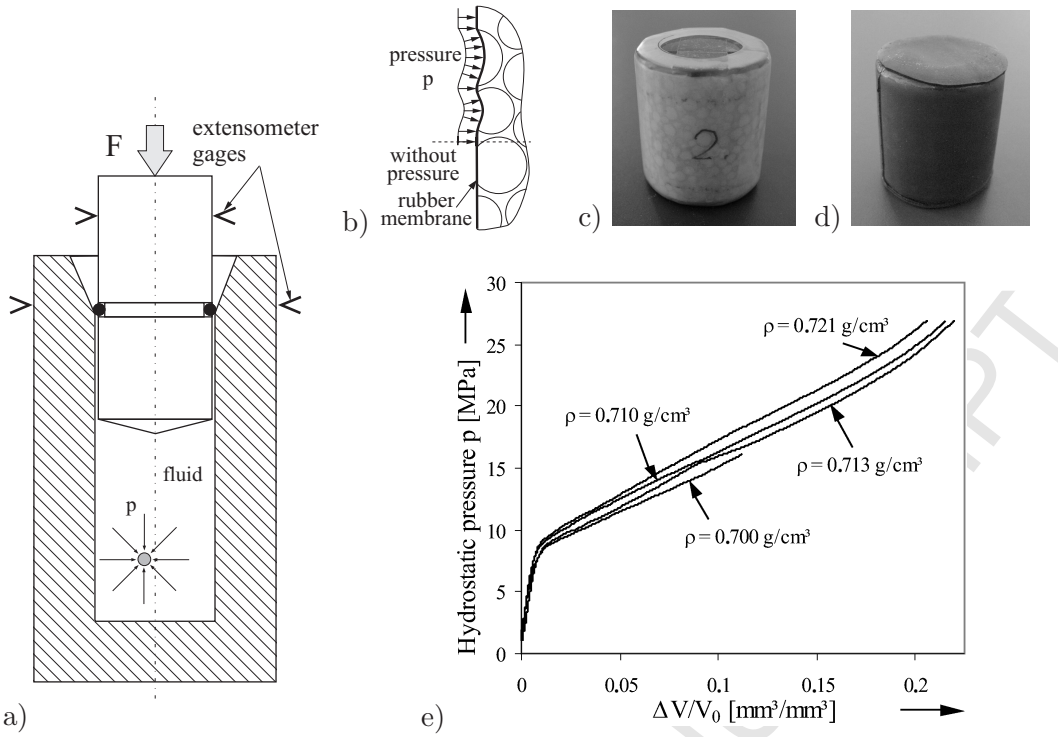

Fig. 8. Hydrostatic pressure test: a) Experimental setup schematically; b) Specimen surface beneath the wrapping; c) First layer of the wrapping; d) Second layer of the wrapping; d) Hydrostatic pressure volumetric strain curves

were identical. Hydrostatic pressures up to 30MPa are possible with the device. The cylindrical specimen dimensions were 35mm in diameter and 36mm in height. The stamp was loaded with a constant velocity ($\dot{\varepsilon}_{start} = 1 \cdot 10^{-3} s^{-1}$).

A wrapping protected the porous specimen against infiltration with the fluid. The wrapping was flexible to ensure the hydrostatic loading of the specimen. It consisted of two layers due to the high pressure. The first layer was a flexible heat shrink tube and the second a butyl rubber membrane (Fig. 8c and 8d). The glass granulates on the boundary of the specimen were sliced. These granulates were loaded by the wrapping directly and after break down the flexible wrapping would have infiltrated in the emerging cavity (Fig. 8b). Therefore the sliced granulates were replaced by epoxy resin to avoid this effect.

The volumetric strain of the specimen was directly proportional to the penetration depth of the stamp, which was measured by an extensometer (Fig. 8a). A reference test was required to consider the compliance of the pressure chamber, the sealing, the fluid and the wrapping. For this a steel specimen was used, the stiffness of which is much greater than the stiffness of the cellular composite. The reference specimen had the same dimensions and wrapping as the cellular composite. The volumetric strain, which was measured in the reference test, had to be subtracted from the volumetric strain of the cellular composite

at the corresponding pressure loads. Fig. 8e shows the experimental results. Under hydrostatic pressure the material strength is higher and the slope of the plateau is obviously steeper compared to the uniaxial compression test.

The experimental results are the basis for the description of a yield surface. The initial yield surface (Fig. 9) is determined for a plastic strain of 0.1%. For the description of the yield function the first invariant of the stress tensor $I_1 = \sigma_{ii}$ and the second invariant of the stress deviator $J_2 = \frac{1}{2} s_{ij} s_{ij}$ are used. The yield surface is not symmetrical to the $\sqrt{3J_2}$-axis (von Mises stress). Therefore a yield function [14] with the form

$$F = f(I_1, J_2) - k^2 = a_0 \cdot I_1^2 + a_1 \cdot I_1 + J_2 - k^2 = 0 \tag{1}$$

is necessary for a good approximation of the experiments (Fig. 9). If the yield function would contain only I_1^2 (without I_1), the elliptical function would be symmetrical to the $\sqrt{3J_2}$-axis [15], which is not sufficient for the material behaviour under consideration. The material law *MAT_BILKHU_DUBOIS_FOAM in the commercial FEM software LS-DYNA, based on [10], uses a yield function like equation (1).

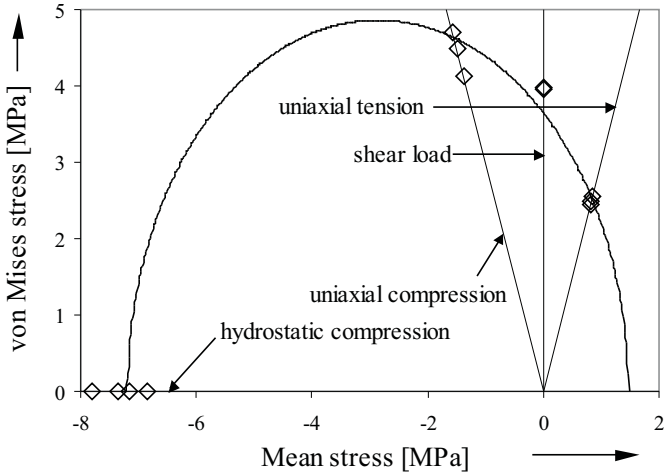

Fig. 9. Initial yield surface of the celluar composite with experimental results

To investigate the strain rate sensitivity of the material, additional uniaxial compression tests were carried out. The experiments were conducted on an Instron VHS High Strain Rate System (VHS 50/20), a test rig which is capable of doing tests at velocities up to $20m/s$ (Fig. 10a). The test rig and data acquisition was controlled by the test software (High Rate, Instron). For the test at the strain rate $\dot{\varepsilon} = 0.01s^{-1}$ a sampling rate of 50Hz was used, for the strain rates $\dot{\varepsilon} = 1s^{-1}$ and $\dot{\varepsilon} = 10s^{-1}$ data was acquired with a sampling rate of 20kHz and the test at the strain rate $\dot{\varepsilon} = 100s^{-1}$ was sampled with a rate of 2MHz. It has to be noted, that due to the impact at high velocities of the piston onto the crosshead, vibrations are induced into the test rig. These vibrations will result in an oscillation of the recorded force signal. Therefore, to

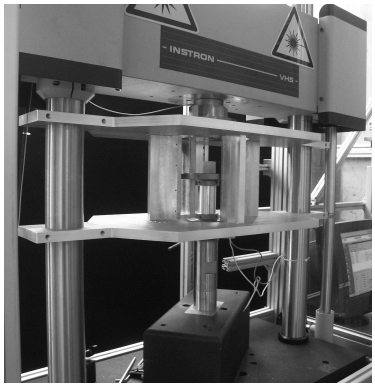

a)

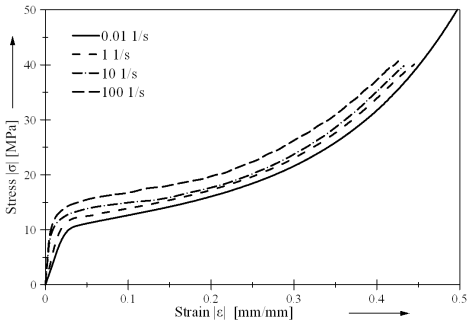

b)

Fig. 10. Strain rate sensitivity a) Test rig (Instron VHS 50/20) b) Stress strain diagramme

acquire reasonable data, suitable filtering techniques have to be used. In this case the data of the experiment with the strain rate $\dot{\varepsilon} = 100s^{-1}$ was filtered (digital lowpass filter, type Butterworth, threshold frequency 4kHz). Strain rate hardening can be observed (Fig. 10b). The stress level of the material is increasing with testing speed. This may be caused by the strain rate sensitivity of the polymeric matrix material [1] .

3 Experimental data at large deformations

In order to investigate the development of the yield surface under large deformations, the experimental data has to be expanded until the beginning of the compaction phase [16] (see Fig. 12).

To acquire additional points of the yield surface, a testing device was used, which blocked the transverse strain of the specimen and measured the resulting transverse force as well as the longitudinal force. The specimen (35mm $\times$ 35mm $\times$ 35mm) was fitted between four moveable rams (Fig. 11a) which constrained the lateral deformation. To measure the transverse force strain gauges were applied on the bolts connecting the rams to the outer walls. The testing device was placed in an electro-mechanical universal material testing machine (Zwick; Z 250), which provided the longitudinal loading of the specimen with a punch (Fig. 11b). In the following this experiment will be called

[1] As it was impossible to install a extensometer, like the Zwick MultiXtens to the VHS, the displacements were measured by the piston movement. Although the piston movement is a suitable means of measuring the displacements in the elasto-plastic range of the material, it lacks the needed accuracy for the measurement of the small displacements in the elastic range of the material. Therefore the strain rate influence on the quasi elastic properties of the material will not be discussed in this paper.

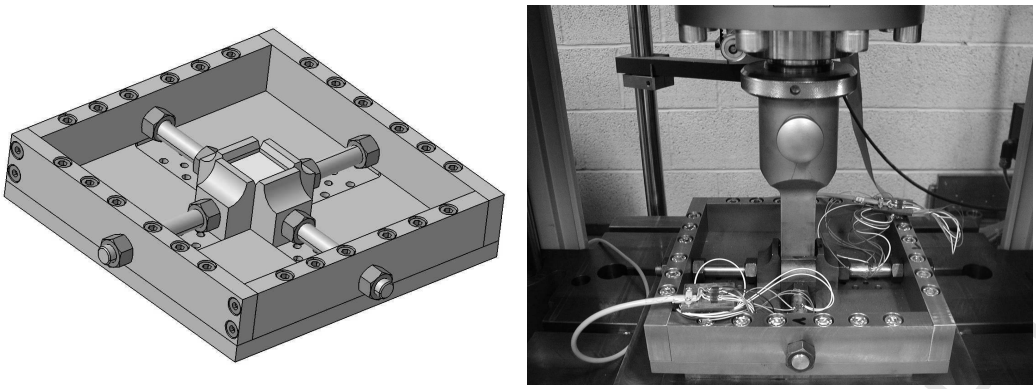

a) b)

Fig. 11. Testing device for multiaxial experiments: a) Schematic view; b) Device in universal testing machine

quasi triaxial. Two of the four rams could be dismantled. With this configuration the lateral deformation in one direction was left free, while the other one was blocked. This test setup will be called quasi biaxial test in the following.

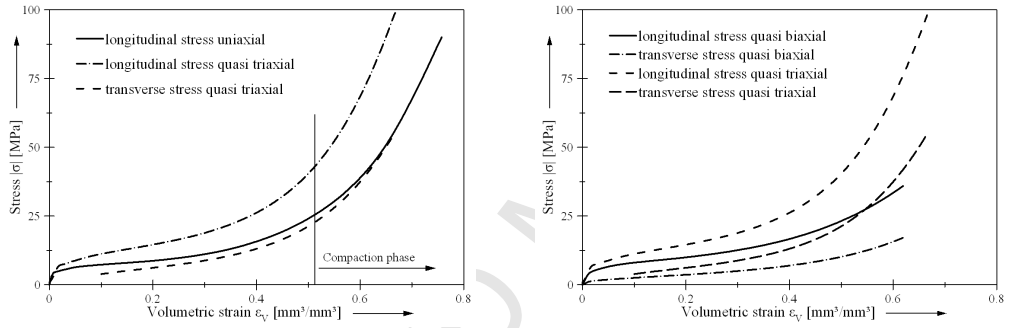

a) b)

Fig. 12. a) Comparison between uniaxial and quasi triaxial tests b) Comparison between quasi biaxial and quasi triaxial tests

As a result of the blocked lateral deformation the longitudinal stress of the quasi triaxial experiment (mean values of four specimens) is increased compared to the uniaxial experiment (Fig. 12a). In addition a significant stress in the transverse direction was measured. This is a result of the non-zero Poisson's ratio of the composite material within the plastic range. Fig. 12b shows a comparison between the quasi triaxial experiment (both lateral deformations were blocked) and the quasi biaxial experiment (only one lateral deformation was blocked, here mean values of two experiments). The stresses of the biaxial test are lower, because only one lateral deformation was constrained. The results in Fig. 12 are plotted over volumetric strain ε_V (with: $\varepsilon_V = -ln\left(\frac{V}{V_0}\right)$), according to [10].

These tests can be performed up to volumetric strains ε_V higher than 0.6, that is into the compaction phase of the material. For the description of the

yield surface it would be beneficial, if the data for the hydrostatic test were also available for these large strains. As the hydrostatic test rig was not fit for the corresponding high pressures, a numerical FEM model of the material on the mesoscopic level was developed [2, 9] (Fig. 13b) in order to simulate the test. Due to the low strength of the granulate under investigation, it has only a small influence on the material behaviour at large strains [9] and therefore was neglected in this model. The polyamide matrix was modeled with 3D tetrahedral elements using a piecewise linear elasto-plastic material behaviour and an element erasing criterion. The FEM programme LS-DYNA was used for the simulation. The mesoscopic model shows a similar behaviour as the experimental curve (Fig. 13a), available up to volumetric strains of 0.3. The offset of the two curves may be due to the simplifications in the numerical model. Nevertheless the general behaviour is the same and it may be found appropriate to extrapolate the experimental data into the range of larger strains by means of adding an offset to the numerical data (Fig. 13a).

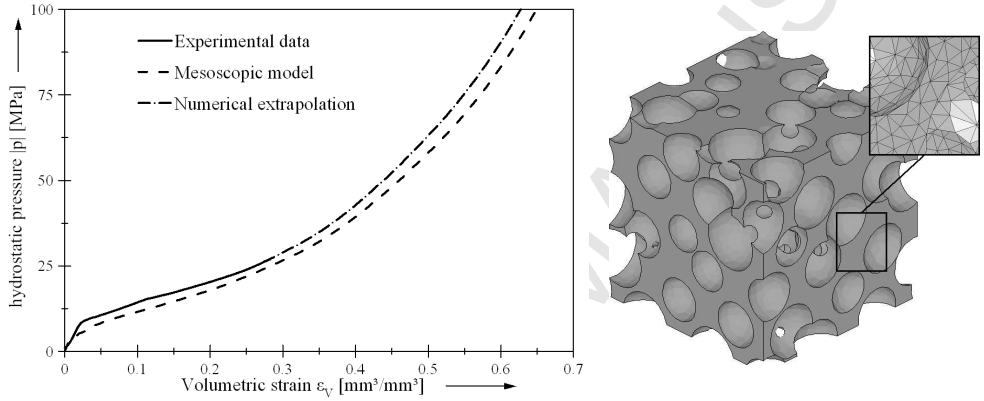

a) b)

Fig. 13. a) Hydrostatic data extrapolated with a numerical model; b) Numerical model

The results gathered in the uniaxial tension, the uniaxial compression, the quasi biaxial compression, the quasi triaxial compression and the hydrostatic pressure tests are plotted into the invariant space (von Mises equivalent stress versus mean stress, Fig. 14). Each of the symbols represents an experiment (or data obtained by numerical simulation) [2] at a certain level of deformation. For this diagramme the individual experiments are compared at levels of the same volumetric strain. The initial yield surface shown in Fig. 9 is also drawn. The material shows a pronounced hardening behaviour, that is with increasing volumetric strain, the corresponding absolute values of the mean stress and the von Mises equivalent stress increase significantly.

[2] All data points are evaluated from experimental data, only the two values for hydrostatic compression at volumetric strains of 0.4 and 0.5 are extrapolated data

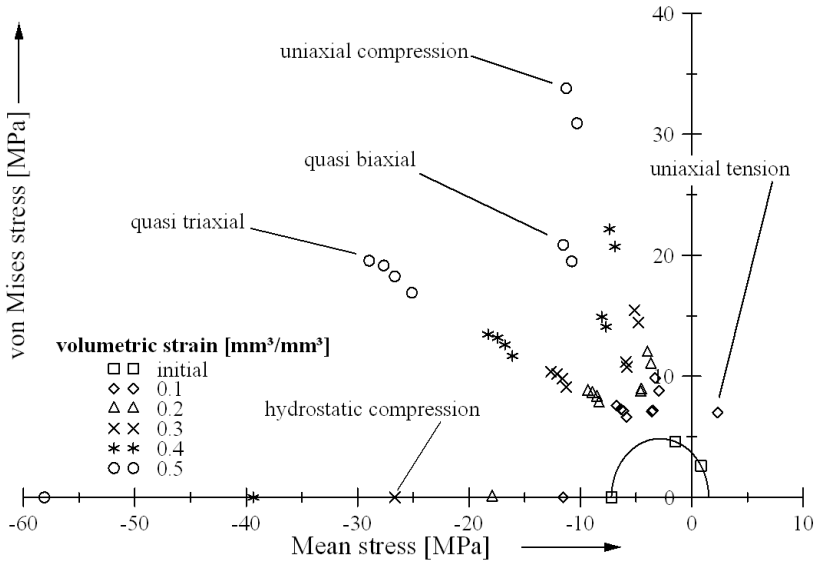

Fig. 14. Results in invariant space

4 Derivation of a continuum model for large deformations

Although the modeling on the mesoscopic level of the material is possible [9], it is only suitable for basic research of the material, because it would lead to very large FEM-models for larger components, which are almost impossible to handle even on modern computers. Therefore a model at the macroscopic level is needed, which represents the material as a continuum for a specific representative element volume and is suitable for application in standard FEM codes. In this paper the focus is on the yield surface of such a material model. For further information concerning material modeling the reader is referred to literature (e.g. [10, 15, 17, 18]). Due to the different diameters and the purely statistical distribution of the granulates during the manufacturing of the material, an isotropic behaviour of the material is assumed in the following, which could be proved by experiment [1].

In literature different shapes of the yield surface have been proposed [15, 19, 20, 21]. The most common formulation is that of an ellipsoid in the principal stress state [22]. An elliptical yield surface can be described with an equation like (1). It can be seen in Fig. 14 that for this material a fitting of the yield curve at higher volumetric strains is not possible with an elliptic curve.

Different approaches may be used to compare states of multiaxial stress on the yield curve. In case of this specific material, a better fitting to elliptical curves is achieved by using the specific plastic deformation energy as a criterion. The increment of the specific plastic deformation energy can be calculated as

$$dw^p = d\varepsilon_{ij}^p \sigma_{ij} \tag{2}$$

where $d\varepsilon_{ij}^{p}$ denotes the increment of the plastic strain tensor and σ_{ij} represents the current stress tensor. The increment of the plastic strain tensor can be calculated by

$$d\varepsilon_{ij}^{p} = d\varepsilon_{ij} - d\varepsilon_{ij}^{e} \ . \tag{3}$$

In this equation $d\varepsilon_{ij}$ denotes the increment of the total strain tensor and $d\varepsilon_{ij}^{e}$ represents the increment of the elastic strain tensor, which can be determined by

$$d\varepsilon_{ij}^{e} = \frac{1+\nu^{e}}{E} \cdot d\sigma_{ij} - \frac{\nu^{e}}{E} \cdot d\sigma_{kk} \cdot \delta_{ij} \ . \tag{4}$$

E is Young's modulus, ν^{e} is the elastic Poisson's ratio and δ_{ij} denotes the Kronecker symbol. Due to the damage to the granulates and the matrix material in the ongoing deformation Young's modulus is not a constant value, but changes. To investigate the quantity of the change, uniaxial experiments where conducted, in which the specimen was loaded and unloaded repeatedly. Due to the inhomogeneous structure of the material, a superposition of different effects results in the behaviour of the material shown in Fig. 15a. The cellular build-up of the material leads to bending and buckling of the cell walls during the loading process. The stresses induced into the matrix material by these deformations result in an elastic relaxation during the unloading process. These effects are overlapped by the viscoelastic behaviour of the matrix and the damage of the granulates. To separate these effects and evaluate the influence on the elastic behaviour, further investigations have to be conducted. In this paper, the change of the Young's modulus of the compressed material is of relevance. Therefore, the following approach was chosen: A modulus was approximated to the elastic unloading path of the specimen (Fig. 15a). The approximated modulus will be called current Young's modulus in the following. Fig. 15b shows the results of this investigation in values of relative Young's modulus. The relative Young's modulus in this case is the relation of the current Young's modulus E to the initial Young's modulus E_0 ($E_{rel} = \frac{E}{E_0}$). It can be observed, that at first, E_{rel} falls, which corresponds to the loss of stiffness due to the break of the granulates. After the current Young's modulus has reached approximately 62% of the original Young's modulus value, E_{rel} starts to increase to values which are even higher than the initial value ($E_{rel} > 1$). This seems to be plausible, since the voids of the materials are mostly closed and the material behaves more and more like a solid matrix.

In Fig. 16 the experimental data gathered in section 3 is plotted at constant values of specific plastic deformation energy obtained by equation (2). The initial yield surface, described in section 2, is plotted in the diagramme as well. The ellipses are calculated using equation (1) and are fitted to the uniaxial, quasi biaxial, quasi triaxial and hydrostatic compression test. For the initial

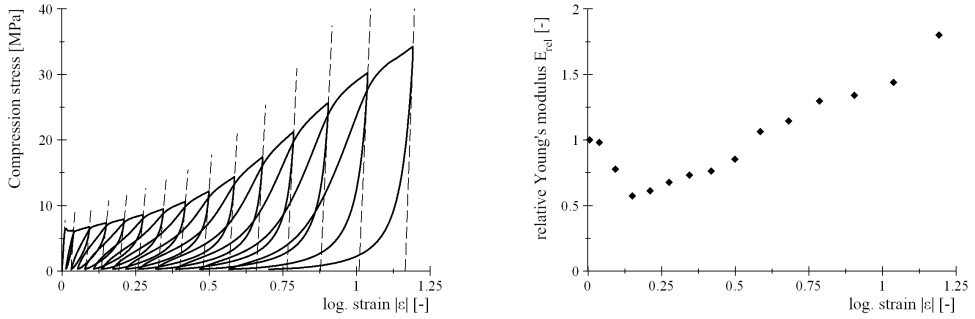

a) b)

Fig. 15. Investigation of compression damage: a) Uniaxial cyclic loading and unloading; b) Relative Young's modulus

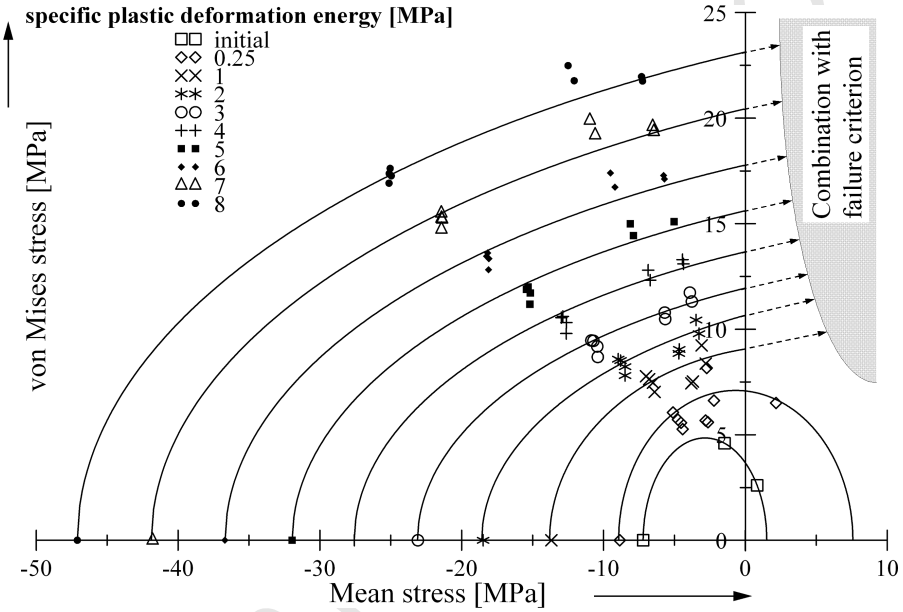

Fig. 16. Invariant space with yield ellipses at constant specific plastic deformation energy

yield surface and the yield surface at $w^p = 0.25MPa$ the uniaxial tension test was used as well. In the uniaxial tension test, the material will fail at $w^p \approx 0.28MPa$ and thus the yield surfaces for $w^p > 0.25MPa$ are not extended into the range of positive mean stress.

Hence, for this specific material the yield condition is given by equation (1). To account for the work hardening of the material, the material parameters a_0, a_1 and k are defined by the evolution of the yield surface, and are dependent on w^p, as described in Fig. 16. Therefore, equation (1) can be written as

$$F = a_0(w^p) \cdot I_1^2 + a_1(w^p) \cdot I_1 + J_2 - k^2(w^p) = 0 \ . \tag{5}$$

The increment of the plastic strain $d\varepsilon_{ij}^{p}$ can be calculated using the flow rule

$$d\varepsilon_{ij}^{p} = d\gamma \cdot \frac{\partial g}{\partial \sigma_{ij}} \ . \tag{6}$$

In this equation $d\gamma$ is the proportionality factor and g is the plastic potential function. For a cellular material, such as the presented composite material, the plastic potential function

$$g = \sqrt{3J_2 + \frac{1}{2}I_1^2} \tag{7}$$

was selected according to [23], which results in a nonassociated flow rule.

To represent the failure of the material a failure criterion for the tensile domain as shown in [12] may be added to the material model [3] . The elements are deleted from the FEM model, when a certain level of the first principal strain is reached. Due to the fact, that failure happens at different stages of deformation in the tension and the compression domain, the strain state has to be determined by checking whether the volumetric strain is positive or negative.

This continuum material model was implemented into the FEM code LS-DYNA (version 970, revision 5434a) as a user defined material routine on the basis of the *MAT_BILKHU_DUBOIS_FOAM material model. The effect of the variation of Young's modulus was neglected in the continuum model, because it is supposed that its influence is small at large plastic deformations, for which this model was derived. In order to show the improvement of the result quality in simulations of the described material using the specific plastic deformation energy, the quasi triaxial test was modeled. In the first simulation, the described material model was used for the specimen. In the second simulation *MAT_BILKHU_DUBOIS_ FOAM in its original version was used, which uses the volumetric strain as hardening criterion (see Fig. 14).

The described material model is capable of modeling the complex multiaxial state of stress in the quasi triaxial test (Fig. 17a). This yields in a reasonable fitting of experiment and simulation both in longitudinal and transversal direction. The simulation using the volumetric strain as hardening criterion (Fig. 17b) shows a different result. As would be expected from Fig. 14, experiment and simulation are matching well as long as the deformation of the specimen is moderate. The results are starting to deviate, when a certain level of volumetric strain (in this case $\varepsilon_V \approx 0.4$) is reached (Fig. 17b).

[3] The failure criterion in Fig. 16 is a basic illustration and not an exact graphical representation of the described procedures.

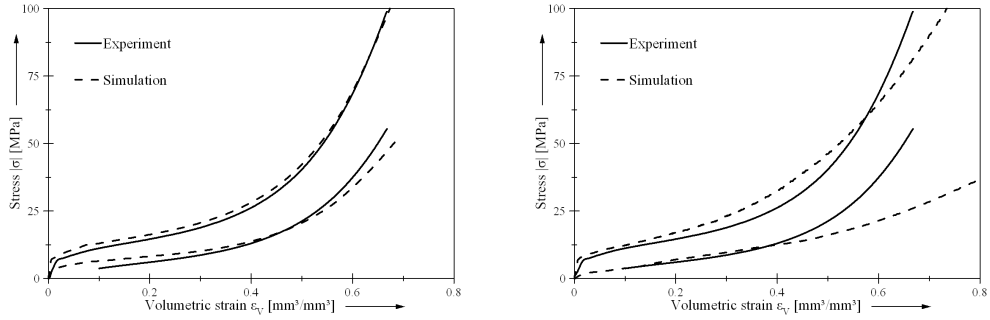

a) b)

Fig. 17. Simulation of the quasi triaxial experiment: a) Described material model b) *MAT_BILKHU_DUBOIS_ FOAM (original version)

5 Application: A crashbox under quasi-static compression load

A crashbox under quasi-static compression load was investigated. The crashbox consisted of a steel shell (DC01, thickness 0.8mm) and a core (thickness 14mm; Fig. 19a) of the presented cellular composite with cast polyamide and glassfoam granulates. Fig. 18 shows the material behaviour of the steel DC01 under uniaxial tension load. Steel shell and core were glued together with an epoxy resin. The two component epoxy resin $L285/H286$ had a tensile strength of approximately $75MPa$.

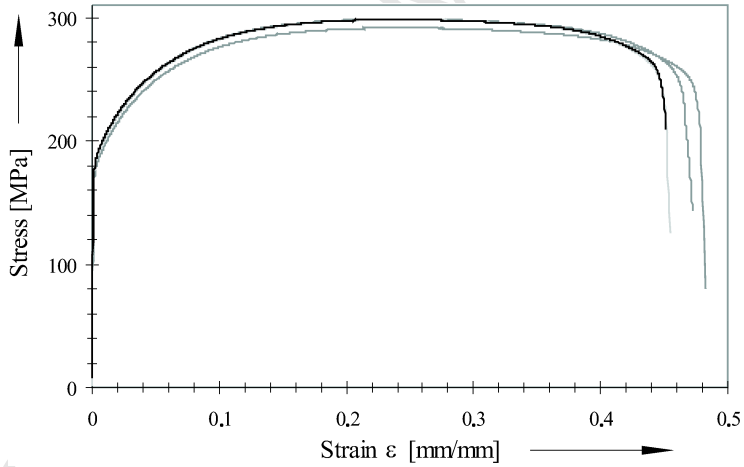

Fig. 18. Stress strain curve of the steel DC01

Repeated unloading allowed the documentation of deformation during the uniaxial compression test. The unloading curves are not included completely in Fig. 19b to improve the clearness. The force-displacement characteristic is relatively homogeneous up to a compression of 100mm. The force variation along the displacement axis corresponds clearly with the buckling characteristics of the crashbox (Fig. 19b). The cellular composite core buckled periodically. The

fracture of the cellular composite started at the tension side of the buckle. The coherence of the core material did not fail completely during the test. At the beginning of the deformation, a force level between approximately 50kN and 75kN was measured. At approximately 90mm deformation, the inner buckles of the core had contact. From this point on, the force displacement curve rose at a progressive rate.

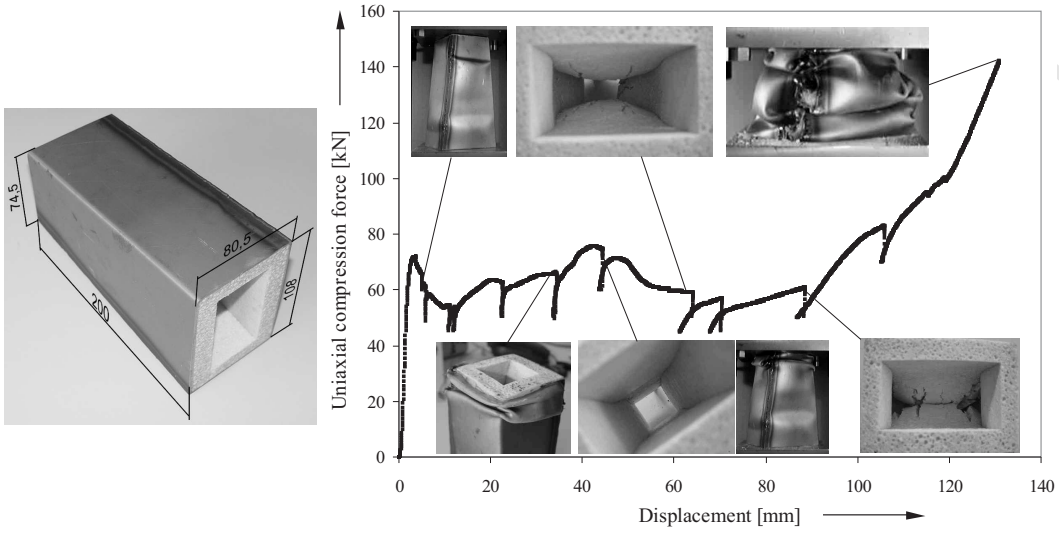

a) b)

Fig. 19. Crashbox - uniaxial compression test: a) crashbox dimensions; b) force-displacement curve of the quasi-static test

The crashbox with the composite core had a weight of $939g$. A pure steel crashbox with the same weight would have a sheet thickness of 1.8mm. Because a sheet with the desired thickness was not available, two crashboxes with a sheet thickness of 1.5 mm and 2.0mm respectively were investigated. For a comparison of the different crashboxes the specific energy absorption

$$e = \frac{\int_{\bar{s}_0=0}^{\bar{s}} F ds}{m_{crashbox}} \tag{8}$$

and the crush force efficiency

$$\eta = \frac{\int_{\bar{s}_0=0}^{\bar{s}} F ds}{F_{max}\left(\bar{s} - \bar{s}_0\right)} \tag{9}$$

according to [24] were used. Fig. 20 shows the comparison of the crashboxes with the crush force efficiencies for $s = 100mm$. For the pure steel crashboxes local force maxima were selected for this special comparison, because the first peak could be reduced by various techniques, e. g. corrugations. The

crashbox with a core of cellular composite showed the highest specific energy absorption, $6.64 kJ/kg$ in relation to $5.36 kJ/kg$ for the 2mm steel shell. Due to the pronounced force peaks of the pure steel shell solutions, the crush force efficiency of the crashbox with a core was better, 0.81 in relation to 0.69 and 0.59 respectively. An efficiency of 1 would be the ideal solution resulting in a constant force displacement diagramme.

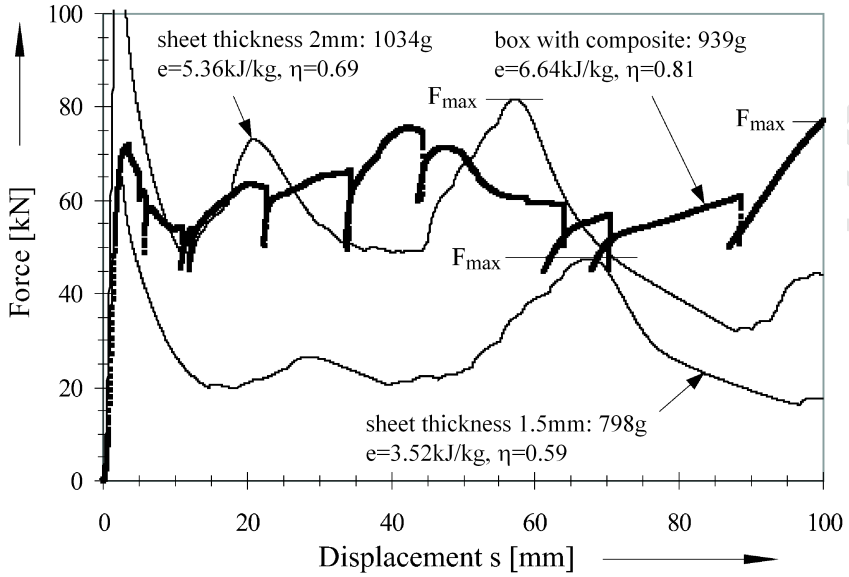

Fig. 20. Force versus displacement diagramme of the crashbox with and without the core out of cellular composite

A FEM model of the described crashbox was developed for simulation using HyperMesh (version 8.0) as a pre-processor and solved with LS-DYNA (version 970, revision 5434a with the described user defined material model). The undeformed and deformed shapes are shown in Fig. 21. Because of the quasi-static conditions of the experiment, only the quasi-static parameters of the materials were used. Because of the explicit formulation of the used solver, it has to be ensured that the kinetic energy is negligible compared to the total energy of the model for a suitable representation of the quasi-static test. Fig. 21a shows the used FEM model of the crashbox. For the steel shell, the material model *MAT_PIECEWISE_LINEAR_PLASTICITY and Belytschko-Tsay shell elements with a size of approximately 3mm were used. The core was modeled using the described material model and solid hexaedral elements with one integration point. Due to the under integrated solid formulation of the elements, a hourglass control using the Flanagan-Belytschko stiffness approach was used. A comparison of the force-displacement curve (Fig. 22) shows similar load levels. To improve the repeatability of the experiments and correlation between experiment and simulation, corrugations in the shell to trigger the deformation are required. Note: The onset of cracks in the core on the macroscopic level begins at deformations of about 50 - 60mm (see also Fig. 19). Therefore the tensile failure of the material can be neglected up to

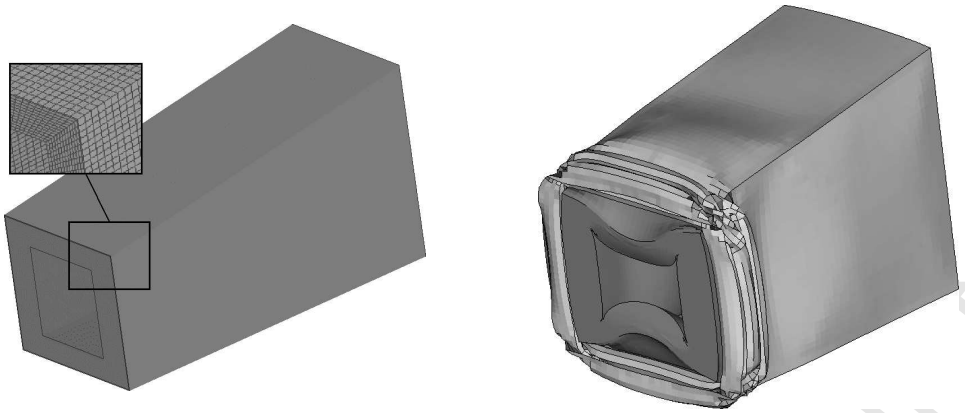

a) b)

Fig. 21. Crashbox: a) Before and b) After compression (displacement ≈ 60mm)

this point. For simulations beyond that point, a failure model, as described in [12] has to be implemented.

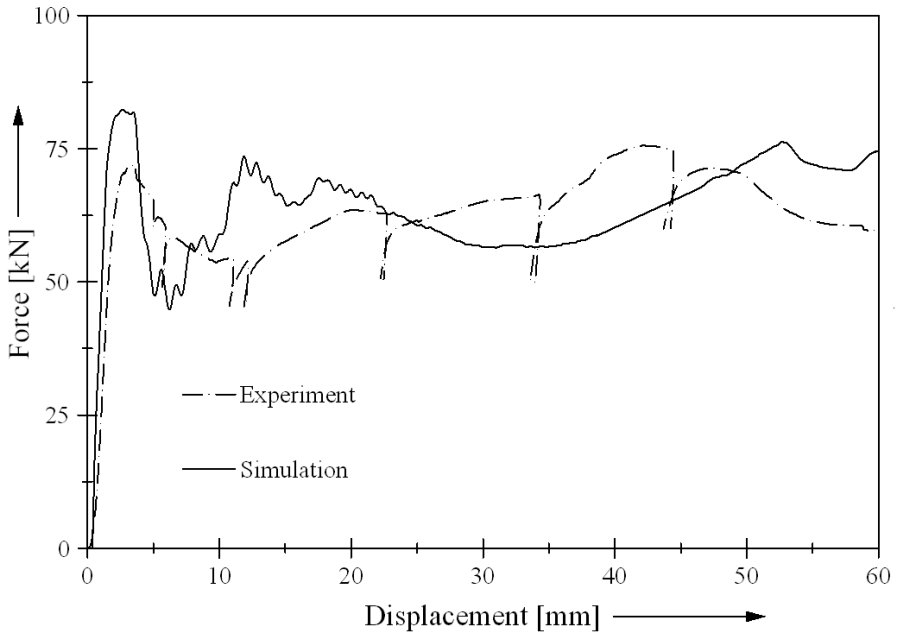

Fig. 22. Force versus displacement diagramme of the crashbox

The investigations of the crashbox were conducted in a quasi-static environment, as the focus of this paper is on the development of a yield surface of the material and not on other effects like strain rate sensitivity. In a test under higher strain rates like the AZT Test ([25], impact velocity: 16km/h), strain rate effects (see Fig. 10) should be included, as done e.g. in [12], where the yield surface is scaled by appropriate factors, corresponding to the current strain rate.

6 Conclusion

A novel cellular material made of porous glass granulates embedded in a polyamide matrix has been investigated in this paper.

The elastic-plastic behaviour of the material up to large deformations was investigated by various experiments. The multi-axial state of stress plays a major role in the onset of plastic yielding. E.g. the blocking of lateral deformations during uniaxial compression results in significant increase of the compressive stress and in stresses in the lateral direction as well. This means that lateral contraction must not be neglected for this type of materials. The yield surface can be represented with an elliptical yield function. This will hold for larger deformations as well, if the specific plastic deformation energy is used as the evolution parameter for the yield surface.

The representation of the yield surface has been implemented in a material model for FEM simulations. It has been shown that the behaviour under a multi-axial state of stress can be simulated.

Using a crashbox under quasi-static loading as an example it could be shown that the cellular material may be beneficial for such applications and that FEM simulation of component behaviour is possible with the proposed material representation.

Besides this, it would be beneficial to incorporate into the material model additional effects like strain rate sensitivity, material failure, variation of Young's Modulus and Poisson's ratio over deformation history, which were not the scope of this paper. Part of this was shown in previous papers [12, 1] or is the scope of current research.

7 Acknowledgements

The presented investigations were made within the project IMVAL (**I**nnovative **M**ineralschaum **V**erbund **A**pplikationen für den **L**eichtbau). The authors thank the German "Bundesministerium für Wirtschaft und Technologie" for the encouragement of the project in the framework of the promotion programme InnoNet and all the partners for their specific support.

References

[1] Dallner, R.; Bartl, F.; Meyer W.: Final report of the research project "IMVAL", Institut für Angewandte Forschung, University of Applied Sciences Ingolstadt, 2007

[2] Huber, O.; Klaus, H.; Dallner, R.; Bartl, F.; Eigenfeld, K.; Kovacs, B.; Godehardt, M.: Herstellung und Eigenschaften syntaktischer Metallschäume mit unterschiedlichen Matrix- und Füllmaterialien (Teil I - III), Druckguss Praxis, 1/2006, p. 19-24, 2/2006, p. 69-75 und 5/2006, p. 205-216, Schiele & Schön, 2006

[3] Klaus, H.; Huber, O.: Experimentelle und numerische Untersuchung der Verbundwerkstoffes "Mineralschaumgranulate in Polyamidmatrix" im elastischen Bereich, in: Huber, O.; Bicker, M. [Eds.]: 2. Landshuter Leichtbau Colloqium, p. 125 - 135, LC Verlag, Landshut, 2005

[4] Godehardt, M.: Analyse tomographischer Aufnahmen von Polyamidmatrizen mit keramischen Granulaten, Fraunhofer Institut für Techno- und Wirtschaftsmathematik: unpublished test report, Kaiserslautern 2004.

[5] Klaus, H.; Huber, O.; Kuhn, G.: Lightweight Potential of Novel Cellular Spherical Composites, Advanced Engineering Materials, 7/12, 2005, p. 1117-1124, WILEY-VCH, Weinheim, 2005

[6] Klaus, H.; Huber, O.; Kuhn, G.: Materialverhalten eines Kugelverbundwerkstoffes im linear-viskoelastischen Bereich, Technische Mechanik, volume 26, issue 2, 2006, p. 71-84, University of Magdeburg, 2006

[7] Klaus, H.: Charakterisierung, Modellierung und Anwendung zellularer Verbundwerkstoffe im elasto-plastischen Bereich, Dissertation, University of Erlangen-Nuremberg, Oct. 2007

[8] Klaus, H.; Huber, O.: FEM-Modellierung für den Verbundwerkstoff "Mineralschaumkugeln in Polyamidmatrix" im elastischen Bereich, in: Huber O.; Bicker M. [Eds.]: 1. Landshuter Leichbau Colloqium, p. 105 - 114, LC Verlag, Landshut, 2003

[9] Bartl, F.; Dallner, R.; Hartmann, M.; Meyer, W.: Simulation eines neuartigen Mineralschaum-Verbundwerkstoffes für Crash-Applikationen, Conference Proceedings, 23rd CADFEM User's Meeting, 2005

[10] Nusholtz, G.; Bilkhu, S.; Founas, M.; DuBois, P.: A simple elastoplastic model for foam materials, STAP Conference, Alberquerque, 1996

[11] Hallquist, J.: LS-DYNA Theoretical Manual, Livermore Software Technology Corperation, May 1998

[12] Bartl, F.; Dallner, R.; Hartmann M., Meyer, W.: Ein numerisches Werkstoffmodell für Mineralschaumverbundwerkstoffe für crashrelevante Anwendungen, in: Huber, O.; Bicker, M. [Eds.]: 3. Landshuter Leichbau Colloquium, p. 81 - 92, LC Verlag, Landshut, 2007

[13] Huber, O.; et al. 5. Semester: Konstruktion von Versuchsvorrichtungen für die Werkstoffprüfung eines neuartigen Leichtbauverbundwerkstoffes, Konstruktionsarbeit, University of Applied Sciences Landshut, 2004

[14] Mahrenholtz, O.; Ismar, H.: Zum elastisch-plastischen Übergangsverhalten metallischer Werkstoffe, Ingenieur-Archiv, 50, p. 217-224, 1981
[15] Deshpande, V.S.; Fleck, N.A.: Isotropic constitutive models for metallic foams, Journal of Mechanics and Physics of Solids, volume 28, p. 1253-1283, 2000
[16] Bartl, F.; Dallner, R.; Meyer, W.: Experimentelle und numerische Untersuchung ausgewaehlter zellularer Werkstoffe bei höheren Dehnraten, Materialwissenschaft und Werkstofftechnik, 36 (2005), no. 6, p. 254-263
[17] Chen, W.F.; Han, D.J.: Plasticity for Structural Engineers, Springer, New York, 1988
[18] Simo, J.C.; Hughes, T.J.R.: Computational Inelasticity, Springer, New York, 1998
[19] Hanssen, A.G.; Langseth, M; Hopperstad, O.S.; Ilstad, H.: Validation of constitutive models applicable to aluminum foams, International Journal of Mechanical Sciences, volume 43, p. 359-406, 2002
[20] Chen, C.; Lu, T.J.: A phenomenological framework of constitutive modelling for incompressible and compressible elasto-plastic solids, International Journal of Solids and Structures, volume 37, p. 7769-7786, 2000
[21] Wicklein, W.; Thoma K.: Numerical investigations of the elastic and plastic behaviour of an open-cell aluminium foam, Materials Science and Engineering A, volume 297, p. 391-399, 2005
[22] Öchsner, A.: Experimentelle und numerische Untersuchung des elastoplastischen Verhaltens zellularer Modellwerkstoffe, Dissertation, University of Erlangen-Nuremberg, 2003
[23] Bilkhu S.; Founas M.; Nusholtz G.: Material modeling of Structural Foams in Finite Element Analysis Using Compressive Uniaxial and Triaxial Data, SAE Technical Paper 930434, 1993
[24] Hanssen, A.G.; Langseth, M.; Hopperstad, O.S.: Static crushing of square aluminium extrusions with aluminium foam filler, International Journal of Mechanical Sciences, 41, 1999, S. 967-993.
[25] Allianz Zentrum für Technik GmbH: AZT Crashreparaturtest Front (Neuer RCAR Strukturtest - 10°). Allianz Zentrum für Technik GmbH. Internet: http://www.allianz-azt.de/